Attack transient exploration on sopranino recorder with time-domain Near-Field Acoustic Holography method

M. Tahon[a], E. Bavu[a], M. Melon[b] and A. Garcia[a]
[a]LMSSC, CA 3196, CNAM, 2 rue Conté, 75141 Paris Cedex 3, France
[b]LAUM, UMR CNRS 6613, avenue Olivier Messiaen, 72085 Le Mans Cedex 9, France
tahonm@cnam.fr

Directivity of musical instruments have been studied for a long time. In the last decades, there has been a growing interest in imaging methods for the characterization and localization of sound sources. These developments are of great help to study the stationary and transient radiation behaviour of woodwind instruments.
The time-domain Near-Field Acoustic Holography is one of these powerful imaging methods. NAH allows to separate the sources contributions from the different parts of an instrument. One of the advantage of the time-domain holography is to observe acoustic phenomena during transitory states. Most studies on recorder acoustic radiation were conducted during steady state, yet none of them focus on the attack transients. In order to investigate the acoustic radiation of the sopranino recorder, we use a semi-cylindrical microphone array, thus taking advantage of the geometrical symmetry of the recorder. In this study, the imaging method is used for the localization and the characterization of radiating sources on a sopranino recorder played by a performer. The array consists in a 4 angular and 11 longitudinal microphone arrangement. Taking into account the symmetry, the number of measurements points is $2 \times 11 \times 4 = 88$. The recorder is located at the center of the cylindrical array. This study aims at highlighting an acoustic coupling between finger holes, labium and bell during the attack transient. This experiment allows us to validate the experimental protocol: semi-cylindrical array and time domain acoustic holography method for woodwind instruments radiation investigations.

1 Introduction

The knowledge of the radiation properties of musical instruments is of great importance to improve physical models but also for sound recording. Many imaging methods have been used for the characterization of such sound sources. For instance, Meyer and Hansen studied the directivity of several instruments using acoustic holography [1]. Planar holography has also been applied to the guitar radiation [2]. Other acoustical imaging methods have been used for the study of instruments; for example intensity flux lines and directivity diagrams were set up for investigating acoustic radiation of a piano soundboard [3]. Simple microphone recordings with a cylindrical robot were performed by Ehara and Yoshikawa on woodwind instruments such as clarinets [4]. Radiation patterns have also been measured in playing conditions using a surrounding spherical microphone array [5, 6].

Cylindrical Near-Field Acoustic Holography (NAH) has already been implemented to study stationary radiation of sources [7, 8, 9]. Recent developments were carried out to extend stationary imaging techniques to transient sources. Yet, many of the transient holography experiments were carried out using planar coordinates [10, 11, 12, 13].
In this paper, an extension to NAH for transient field imaging is proposed using the cylindrical array geometry. A numerical simulation depicting a very simple case (two monopoles radiating transient signals) is performed to test the proposed algorithm. Finally, the method is applied to the measurement of a sopranino recorder.

2 Theoretical background

2.1 Stationary Cylindrical NAH

It is convenient to describe cylindrical sources and the acoustic field created by them in cylindrical coordinates (r, θ, z). The geometry of the problem is given in Figure 1. Consider a source located in the $r \leqslant r_b$ domain and radiating a harmonic wave at frequency f. The backward propagation problem consists in computing the pressure field at $r = r_b$ from measurements data obtained on a cylindrical array of radius r_m (with $r_m > r_b$). The principle of cylindrical NAH is summarized in Williams book [7] and requires the following steps:

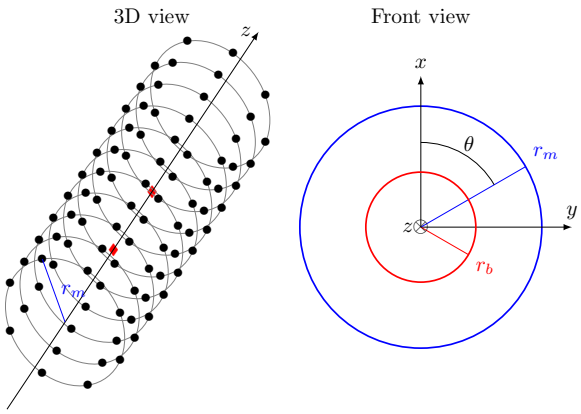

Figure 1: Geometry of interest. •: microphone positions, ♦: monopole positions used for the numerical simulation.

a) Measurement of the pressure field at radius r_m

b) Computation of the time Fourier transforms at radius r_m.

$$\hat{p}(r_m, \theta, z, \omega) = \int_{-\infty}^{\infty} p(r_m, \theta, z, t) e^{-i\omega t} dt \qquad (1)$$

For commodity, the pulsation ω is removed from the following equations.

c) Computation of the spatial Fourier transforms in θ and z of $p(r_m, \theta, z)$:

$$\hat{P}_n(r_m, k_z) = \frac{1}{2\pi} \int_0^{2\pi} d\theta \int_{-\infty}^{\infty} \hat{p}(r_m, \theta, z) e^{-ik_z z} e^{-in\theta} dz \qquad (2)$$

d) Multiplication by the inverse propagator $G_n(k_r, r_m, r_b)$, with $k_r = \sqrt{k^2 - k_z^2}$

$$\hat{P}(r_b, k_z) = \hat{P}_n(r_m, k_z) \times G_n(k_r, r_m, r_b) \qquad (3)$$

e) Computation of the inverse transforms at radius r_b to obtain $p(r_b, \theta, z)$

$$\hat{p}(r_b, \theta, z) = \frac{1}{2\pi} \sum_{n=-\infty}^{\infty} e^{in\theta} \int_{-\infty}^{\infty} \hat{P}_n(r_b, k_z) e^{ik_z z} dk_z \qquad (4)$$

Please note that the computation of the propagator in cylindrical coordinates has two different forms depending on the propagative or evanescent nature of the associated waves. For propagating waves, $k > k_z$, $G_n(k_r, r_m, r_b)$ is expressed in terms of a ratio of Haenkel functions:

$$G_n(k_r, r_m, r_b) = \frac{H_n^{(1)}(k_r r_b)}{H_n^{(1)}(k_r r_m)} \tag{5}$$

For evanescent waves, $k < k_z$, which exhibit an exponential decay with radial distance, the propagator $G_n(k_r, r_m, r_b)$ is expressed in terms of a ratio of modified Bessel functions, with $k_r' = \sqrt{k_z^2 - k^2}$

$$G_n(k_r, r_m, r_b) = \frac{K_n(k_r' r_b)}{K_n(k_r' r_m)} \tag{6}$$

As this problem is ill-posed, regularization techniques need to be used to obtain a reliable solution. In this paper, the Tikhonov filter [14] in its standard form is applied to the backward propagated spectrum.

2.2 Time Domain NAH (TDH)

The extension of stationary cylindrical NAH to time domain NAH can be performed by using the same principle as proposed by Hald [15] for planar holography. This method consists in applying a Fourier transform to the time dependant measurement data, thus obtaining their frequency spectra with equation 1.

Then, after classical cylindrical NAH has been computed, the back-propagated time dependant pressure field at $r = r_b$ is obtained by a simple inverse Fourier transform:

$$p(r_b, \theta, z, t) = \int_{-\infty}^{\infty} \hat{p}(r_b, \theta, z, \omega) e^{i\omega t} dt \tag{7}$$

3 Numerical simulation

3.1 Reconstruction quality indicators

In order to estimate the quality of the holographic reconstruction, three indicators similar to those used by Moulet *et al.* [11] are calculated. Two of them are computed for a given point of the cylindrical source on the whole duration (T_1 and T_2), the last one describes the spatial error among time $E(t)$.

$$T_1(r_{ref}, \theta_n, z_n) = \frac{< p_{ref}(r_{ref}, \theta_n, z_n, t) \times p_{holo}(r_{ref}, \theta_n, z_n, t) >_t}{p_{ref}^{RMS}(r_{ref}, \theta_n, z_n) \times p_{holo}^{RMS}(r_{ref}, \theta_n, z_n)}$$

$$T_2(r_{ref}, \theta_n, z_n) = \frac{\left| p_{ref}^{RMS}(r_{ref}, \theta_n, z_n) - p_{holo}^{RMS}(r_{ref}, \theta_n, z_n) \right|}{p_{ref}^{RMS}(r_{ref}, \theta_n, z_n)}$$

$$E_n(t) = \frac{\sqrt{< \left[p_{ref}(r_{ref}, \theta_n, z_n, t) - p_{holo}(r_{ref}, \theta_n, z_n, t) \right]^2 >_s}}{< p_{ref}^{RMS}(r_{ref}, \theta_n, z_n) >_s}$$

Where $<>_t$ (respectively $<>_s$) is the time (resp. spatial) averaged value. Perfect reconstruction leads to $T_1 = 1$, $T_2 = 0$ and $E_n(t) = 0$.

3.2 Simulation with two monopoles

In order to validate the time domain algorithm, a numerical simulation is performed with a set-up similar to the experimental one. The first [resp. the second] source is located at ($r_1 = 1.4$ cm$, 0, z_1 = 14$ cm) [resp. at ($r_1, 0, z_2 = 20.8$ cm)]. As the player starts blowing at $t = 0$, the first [resp. the second] source radiation starts at $t_1 = z_1/c$ [resp. at $t_2 = z_2/c$]. At low frequencies, finger holes are modelled by monopole sources. The impulse response of each sources is given by:

$$p(R_i, t) = \frac{\delta(R_i/c - (t - t_i))}{4\pi R_i} * s(t) \text{ with } i = 1, 2 \tag{8}$$

Where c is the sound celerity in air and
$R_i = \sqrt{(x - x_i)^2 + (y - y_i)^2 + (z - z_i)^2}$.
The numerical simulation is performed with Matlab. The signal $s(t)$ radiated by the monopole is a Gaussian pulse of 0.1 ms full width at half-maximum. The measurements are simulated with a 64×64, 30 cm length microphone array. The time sampling frequency is set to $F_s = 32768$ Hz. Because finger holes are modelled as impulse punctual sources, the influence of reflection of the acoustic wave on the recorder is not taken into account.

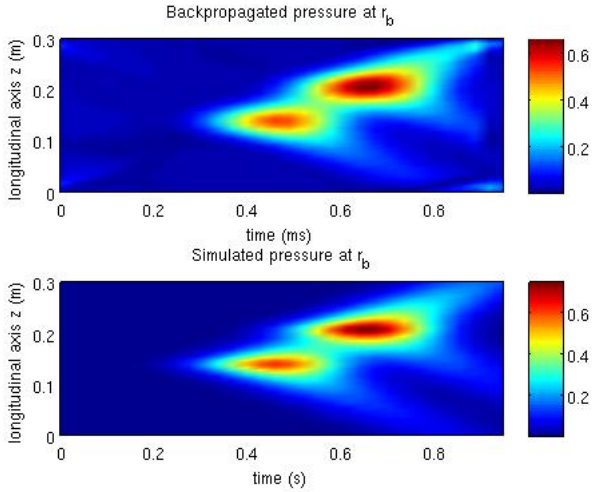

Figure 2: Distribution of back-propagated and simulated pressure (in A.U.) at $r_b = 3$ cm for $\theta = 0$, among the longitudinal and time axis

Figure 2 shows that both back-propagated and theoretical pressure maps at $r = r_b$ have similar shapes in the (z, t) domain. Error criteria are plotted in Figure 3. One can see that magnitude (T_2) errors are more important where the sources are located ($\theta \approx 0$) even if both simulated and back-propagated magnitudes have similar maxima (see Figure 2). The shape error (T_1) is constant among the longitudinal axis. The maximum error surrounds the sound sources at $\theta \pm \epsilon$ but at $\theta \approx 0$ (source location), the T_1 is minimum. The E_n criteria remains low with a $E_{max} < 0.003$ but increase at the final times. The best TDH configuration which gives minimum errors, is a compromise between filtering parameters and the back-propagation distance. Now that the algorithm has been validated with simulated sources, the next steps consists in applying it to a real recorder.

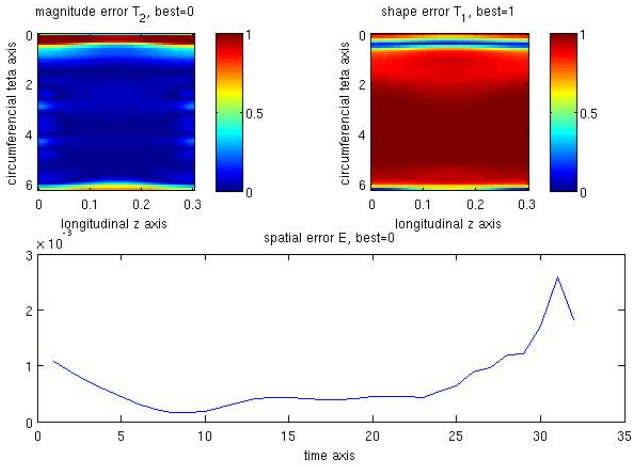

Figure 3: Errors obtained on simulation: T_1, T_2 and E errors.

close as possible to the standard fingerings corresponding to F, B♭ and E♭. The fingerings do not exactly correspond to usual notes in order to keep only zero (F ≈ 700 Hz), one (B♭ ≈ 970 Hz) or two (E♭ ≈ 1250 Hz) open holes. Measurements of the upper regime are also realised. In order to reach the upper regime, the player need to increase the blowing pressure but also to adapt the mouth geometry [16].

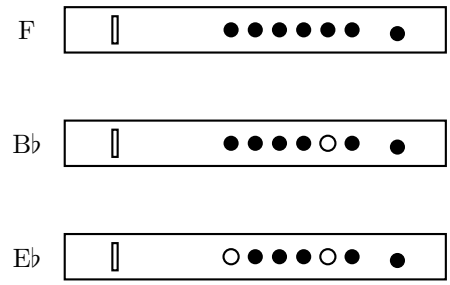

Figure 5: Fingerings used for the experiments

4 Materials and method

4.1 Experimental set-up

The recorder is a sopranino Yamaha which length is 25 cm. The measurement array consists in a 4 angular and 11 longitudinal microphone arrangement. The microphones used are KE4 Sennheiser carefully calibrated in amplitude and phase. In order to take into account the $y = 0$ plane symmetry of the recorder, the finger holes fits with the edge of the array. Adjacent longitudinal [respectively circumferential] microphones are regularly spaced each 3 cm [resp. 45°]. The measurement radius is set to $r_m = 5$ cm, the pressure distribution is estimated at the maximum diameter of the recorder $r_b = 2$ cm. The sampling frequency is set up at $F_s = 32768$ Hz. The player blows in a pipe which is linked to the labium of the recorder. Experiments take place in an anechoic room. Figure 4 shows the experimental set-up.

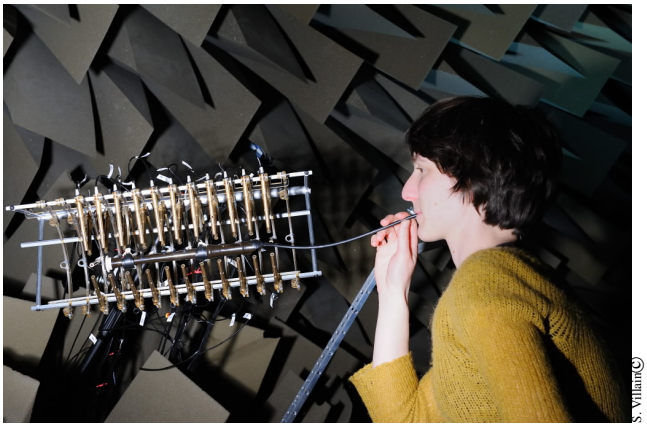

Figure 4: Experimental set-up.

4.2 Method

In order to study spatio-temporal events, different configurations have been experimented. The two most common articulation syllables are applied to the recorder: “t” and “d”. Three different fingerings are chosen to be as

5 Results

NAH is applied to the measurements at radius $r_m = 5$ cm, then the acoustic pressure is back-propagated at the radius $r_b = 2$ cm. The back-propagated pressure is plotted among the longitudinal axis (z) according time at four circumferential (θ) positions (corresponding to microphone positions). The labium is located at $z_l = 4$ cm (microphones 2 and 3), the B♭ finger hole is located at $z_h = 17$ cm (microphones 7 and 8) and the bell is located at $z_b = 26$ cm (microphones 10 and 11). The results obtained with the E♭ are not relevant enough in the sense that the microphone array longitudinal resolution is not enough accurate.

5.1 Directivity results

When the stationary state is reached, some results on the recorder directivity can be obtained. On Figure 6, the labium ($z_l = 4$ cm) mostly radiates at $\theta = \pi/8$ (amplitude 0.15 A.U.) whereas the bell ($z_b = 26$ cm) radiates the same amplitude (almost twice less than the labium: 0.08 A.U.) at all axial positions. These results confirm the fact that the labium is directional whereas the bell is omnidirectional.

5.2 Radiation versus time

Figure 7 shows the back-propagated pressure in function of longitudinal z axis and time. The image focuses on a 3 ms time window. The labium ($z_l = 4$ cm) and the open finger hole ($z_h = 17$ cm) radiations alternate periodically. The biggest period is almost 1.1 ms and the period between two consecutive amplitude maxima is 0.4 ms. The first period approximately corresponds to twice the distance between labium and bell ($219/c \simeq 0.64$ ms). The second period corresponds to the length between labium and the first finger hole ($145/c \simeq 0.42$ ms).

5.3 Upper regime

In fact, the upper regime do not corresponds to a standard note, as the fingerings have been modified. In the present

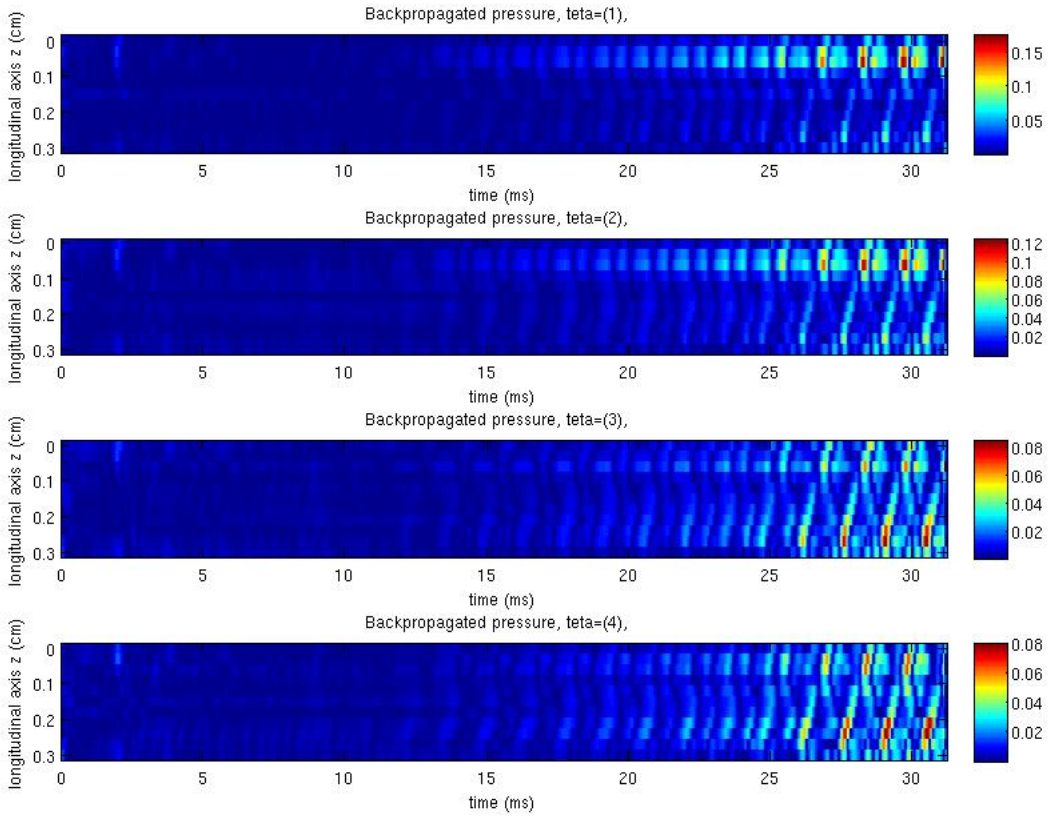

Figure 6: Full radiation (in A.U.). F fingering, attack “t”.

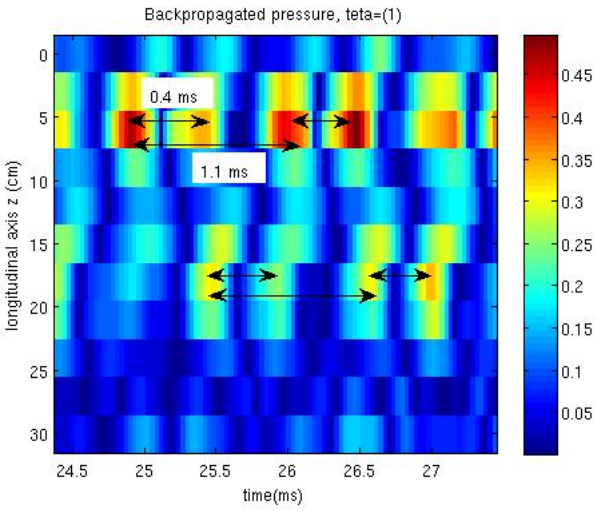

Figure 7: Fundamental regime at $\theta = \pi/8$ (in A.U.). B♭ fingering, attack “t”.

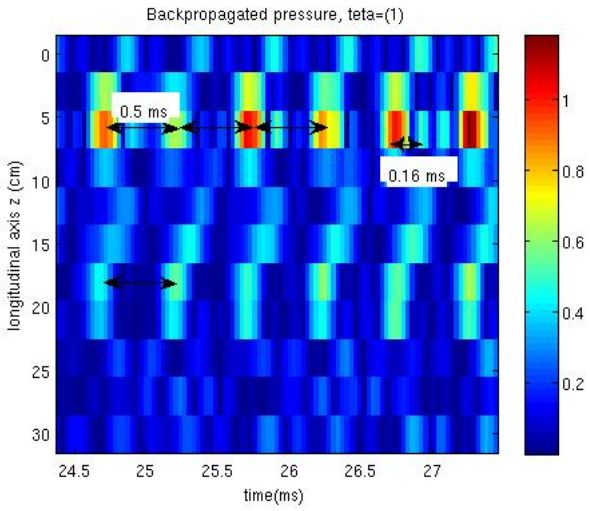

Figure 8: Upper regime at $\theta = \pi/8$ (in A.U.). B♭ fingering, attack “t”.

case, a diphonic sound is heard. On Figure 8, two different periods can be noticed at the labium, and only one at the finger hole. On both the labium and the finger hole there is a period of 0.5 ms ($\approx$ 2000 Hz) which corresponds to octave of the fundamental B♭. At the labium a second period of 0.16 ms ($\approx$ 6200 Hz) exists. Both labium and hole are in phase, showing a different behaviour from the fundamental regime.

5.4 Attack transients

TDH is a powerful tool for analysing the recorder radiation during the first ms after the attack. Figure 9 is a zoom of the Figure 6. The magnitude scale is adapted in order to reveal the acoustic pressure propagation at $\theta = \pi/8$ of the recorder when playing F. The periodicity of the acoustic pressure occurs almost immediately after the attack which occurs at 2 ms. The periodic signal first occurs at the

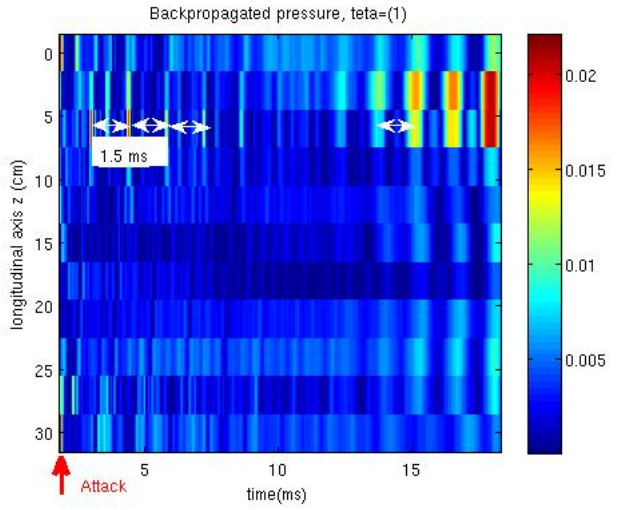

Figure 9: Zoom of Figure 6 at the first time immediately after the attack at $\theta = \pi/8$ (in A.U.). F fingering, attack "t".

labium, and in a second time at the bell. The periodicity is around 1.4 ms what corresponds to a frequency of 714 Hz (note F).
No significant differences between the "t" and the "d" attacks have been noticed. Except that the "t" attack – which is the rudest attack – radiates at the labium with a much higher amplitude than the "d" attack.

6 Conclusion

Cylindrical acoustic holography is interesting for studying the stationary and transient sound radiation of cylindrical wind instruments. This method allows researchers to study spatio-temporal events and to obtain measurements as close as possible to the sound sources. TDH is powerful for exploratory experiments because all spatial, temporal and spectral information are contained in the measurements.
In this paper, TDH is applied to a sopranino recorder. The main results are the visualisation of the directivity of the recorder in stationary state, the visualisation of the radiation of labium, finger hole and bell and their time evolution for both fundamental and upper regime. Some interesting results appear during the transient state: overlapping of different frequencies occur differently in function of the longitudinal z and circumferential θ axis.
This paper offers an acoustic imaging method which could be interesting to study sound sources of cylindrical instruments. Improvements of the method need to be driven, for example in the regularization techniques of the Tikhonov filter. Spatial resolution of the microphone array could be improved using more microphones while temporal resolution can be improved by using a larger sampling frequency. The measurements of acoustic radiation could help improving the knowledge in instrumental acoustics.

Acknowledgments

The authors would like to thank Sarah Poirée for the microphone calibrations and Philippe Chenevez at Cinela for the array design and manufacturing.

References

[1] J. Meyer and U. Hansen, Acoustics and the performance of music: manual for acousticians, audio engineers, musicians, architects and musical instruments makers., Springer (2009).

[2] R. Bader, Acoustic Holography of Musical Instruments using Radiation Directivity Method, 145th Meeting of the Acoustical Society of America (2008).

[3] P. Chenevez, A. Garcia and P. Derogis and R. Caussé, Acoustic Radiation of a Piano Soundboard by Acoustical Imaging Methods., Acta Acustica, Vol. 82, suppl. 1 (1996).

[4] F. Ehara and S. Yoshikawa, Radiation Directionality Measurement of Clarinets Made of Different Wall Material, Forum Acusticum, Budapest, Hungary (2005).

[5] G. K. Behler, M. Pollow and M. Vorlnder, Measurements of musical instruments with surrounding spherical arrays, Acoustics 2012, Nantes, France (2012).

[6] F. Otondo, J.H. Rindel, R. Caussé, N.Misdariis and P. de la Cuadra., Directivity of Musical Instruments in a Real Performance Situation, International Symposium on Musical Acoustics (ISMA), Mexico City, Mexico (2002).

[7] E.G. Williams, Fourier Acoustics – Sound radiation and Nearfield Acoustical Holography, Academic Press (1999).

[8] M. Frechet, Etude du rayonnement d'une flûte à bec par une méthode holographique, Master Thesis, Université du Maine, Le Mans, DEA d'Acoustique Appliquée, (1992).

[9] S.A. Tsysar and Y.D. Sinelnikov and O.A. Sapozhnikov, Characterization of Cylindrical Ultrasonic Transducers using Acoustic Holography, Acoustical Physics, vol. 57, No. 1, pp.94-105 (2011).

[10] O. de La Rochefoucauld, M. Melon, and A. Garcia, Time domain holography: Forward projection of simulated and measured sound pressure field, J. Acoust. Soc. Am., vol. 116 (1), pp.142-153 (2004).

[11] M.-H. Moulet, M. Melon, J.-H. Thomas and E. Bavu, Characterization of non-stationary sources using three imaging techniques, Acoustics 2012, Nantes, France (2012).

[12] O. A. Sapozhnikov, A. E. Ponomarev and M. A. Smagin, Transient Acoustic Holography for Reconstructing the Particle Velocity of the Surface of an Acoustic Transducer, Acoustical Physics, vol. 52, No. 52, pp.324-330 (2006).

[13] J.-H. Thomas, V. Grulier, S. Paillasseur, J.-C. Pascal and J.-C. Le Roux, Real-time near-field acoustic holography for continuously visualizing nonstationary acoustic fields, J. Acoust. Soc. Am., vol. 128 (6), pp. 3554-3567 (2010).

[14] A.N. Tikhonov, A.V. Goncharsky, V.V. Stepanov and A.G. Yagola, Numerical methods for the solution of Ill-Posed problems, Kluwer academic publishers (1995).

[15] J. Hald, Time Domain Acoustical Holography and its application, Sound and Vibration, vol. 35, No. 2, pp.16-25 (2001).

[16] R. Auvray, B. Fabre and P.-Y. Lagrée, Regime change and oscillation thresholds in recorder-like instruments, J. Acoust. Soc. Am., vol. 131, pp.1574-1585 (2012).